Underwater Broadband Acoustic Scattering Modelling Based on FDTD

Shao Jie[1,2], Zhao Weisong[1,2], Jin Xiangjun[1,2], Zhang Xin[1,2], Reza Malekian[3]
*[1]Key Laboratory of Radar Imaging and Microwave Photonics (Nanjing Univ. Aeronaut. Astronaut.),
Ministry of Education, College of Electronic and Information Engineering, Nanjing University of
Aeronautics and Astronautics,
Nanjing, 210016, China
[2]Key Laboratory of Underwater Acoustic Signal Processing, Ministry of Education, Southeast
University,
Nanjing, 210096, China
[3]Department of Electrical, Electronic and Computer Engineering, University of Pretoria,
Pretoria, 0002, South Africa
reza.malekian@ieee.org*

***Abstract*—A modified finite-difference time-domain (FDTD) method is described in this paper. The absorption coefficient which is frequency-dependent is considered, and it is used to compute broadband acoustic scattering model of underwater complex object. The perfectly matched layer (PML) absorbing boundary condition (ABC) is applied to this work. Considering computation and accuracy comprehensively, PML boundary layer number and the attenuation coefficient is set at proper values. Computer Graphics are applied to mesh-generating of the irregular object. A pulse of LFM signal is used to simulate wide-band acoustic scattering field of a circle in 2D and a complex object in 3D. And the scattered acoustic pressure waveforms of some certain points are computed in the calculation field. Results obtained from simulation confirm the high accuracy of the proposed method.**

***Index Terms*—Underwater acoustic scattering, FDTD, absorption coefficient, wide-band signal, complex object.**

I. INTRODUCTION

The finite-difference time-domain (FDTD) method which is presented by Yee in 1966 has been one of the most widely used methods in electromagnetic simulation [1]. In 1995, D. Botteldooren illustrates the use of a numerical time-domain simulation based on the FDTD approximation for studying low- and middle-frequency room acoustic problems [2]. After that, the application of FDTD in room acoustics had great progress in the boundary condition [3], near-to-far-field transformation method [4], and computational speed [5]. In 1996, Wang S. demonstrates the usefulness of the FDTD method in solving underwater acoustic problems [6]. Then, the FDTD method was used to analyse the reflected pulse wave in time domain in shallow water [7]. The above researches all used single-frequency plane wave as an incident wave, only analysed the time and space characteristics of object scattering, and not study the

frequency characteristics. The used absorbing boundary conditions have a larger reflection. And only simple object in 2D is studied.

In this paper, The FDTD method is applied to simulate the sound wave propagation in the time domain with a wide-band signal as an input sound source, and considering the absorption coefficient which is frequency-dependent when the sound propagates through the water. And PML absorbing boundary condition which provides much higher absorption than other previous ABCs in finite-difference methods is used. It improved the simulation performance. Furthermore, the method is applied to some different object to examine the generality of the FDTD technique, from a simple circle in 2D to an irregular object in 3D. Computer Graphics are applied to mesh-generating of the complex object. For the 3D irregular object model, the modelling approach is presented based on the 3DMax. Simulations performed with proposed method can be used to study scattering problem in the ocean as well as approximate scattering models which are more readily incorporated into practical mode.

II. FDTD METHODOLOGY

A. Unified FDTD Formulation

FDTD is first used in electromagnetism, it is based on the Maxwell equations. Consider sound waves propagating in the water. The FDTD formula is based on the basic Euler's equation and the equation of continuity. To derive the finite difference form of these partial differential equations, both time and space need to be discretized. So the calculation field is divided into many grids, which is called Yee cell in electromagnetism. A sketch of the three-dimensional staggered grid system used by the finite-difference method for simulation of the acoustic field is illustrated in Fig. 1.

The following recurrence relations are obtained [6]:

$$u_x^{(n)}(i,j,k) = u_x^{(n-2)}(i,j,k) - \frac{\Delta t}{\mathrm{u}...}[p^{(n-1)}(i+1,j,k) -$$

$$- p^{(n-1)}(i-1,j,k)], \qquad (1)$$

$$u_y^{(n)}(i,j,k) = u_y^{(n-2)}(i,j,k) - \frac{\Delta t}{\mathsf{u}\ldots}[p^{(n-1)}(i,j+1,k) -$$
$$- p^{(n-1)}(i,j-1,k)], \tag{2}$$

$$u_z^{(n)}(i,j,k) = u_z^{(n-2)}(i,j,k) - \frac{\Delta t}{\mathsf{u}\ldots}[p^{(n-1)}(i,j,k+1) -$$
$$- p^{(n-1)}(i,j,k\text{-}1)], \tag{3}$$

$$p^{(n)}(i,j,k) = p^{(n-2)}(i,j,k) - \frac{\ldots c^2 \Delta t}{\mathsf{u}}[u_x^{(n-1)}(i+1,j,k) -$$
$$- u_x^{(n-1)}(i-1,j,k) + u_y^{(n-1)}(i,j+1,k) -$$
$$- u_y^{(n-1)}(i,j-1,k) + u_z^{(n-1)}(i,j,k+1) -$$
$$- u_z^{(n-1)}(i,j,k-1)], \tag{4}$$

where $\ldots$ is the density of the medium, c is the sound speed, u_x, u_y and u_z are components of particle velocity u in x, y and z direction, respectively. u is the space step. Δt is the temporal step size. Subscripts i, j and k are grid step number for x, y and z direction, respectively. Superscript n is a time step number. $p^n(i,j,k)$ represents the pressure field at time $t = n \cdot \Delta t$ and at spatial location $x = i \cdot \Delta x$, $y = j \cdot \Delta y$ and $z = k \cdot \Delta z$. Δx, Δy and Δz are space step for each x, y and z direction. In this work, $\Delta x = \Delta y = \Delta z = \mathsf{u}$.
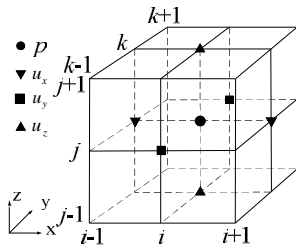

Fig. 1. Three-dimension grid geometry.

Variable Δt must be small enough to ensure stability of the algorithm

$$\Delta t \leq \frac{1}{c}\left(\frac{1}{\Delta x^2} + \frac{1}{\Delta y^2} + \frac{1}{\Delta z^2}\right)^{-1/2} = \frac{\mathsf{u}}{\sqrt{3}c}. \tag{5}$$

So we can use (1)–(4) to update u and p alternately without solving any system of simultaneous equations.

B. Boundary Conditions

The key to solve the acoustic problem with FDTD is to establish proper boundary model. For unbounded problems, the FDTD method requires absorbing boundary conditions (ABCs) to terminate the computational domain. If ABCs are not used, the problem is bounded by the termination of the computational domain which acts like a perfect reflector.

The boundary model consists of impedance boundary model and absorbing boundary model. The impedance boundary model is used to simulate some object in the acoustic field, such as a wall in a room acoustic field [3]. In this work, the boundary of water and the object can use the impedance boundary model.

If we consider a sound wave traveling in a positive x direction (that is, a right boundary), this can be expressed as

$$p = Z_{\mathsf{S}} u_x, \tag{6}$$

where Z_{S} is the boundary acoustic impedance, and u_x denotes the velocity component that is normal to the surface of the boundary.

The locally reacting surface (LRS) model provides a simple basis for model specular reflections, and the LRS concept is captured by two conditions. The first is the boundary condition itself. The second condition is that the multidimensional wave equation holds at the boundary. If these two conditions are met, the corresponding reflection coefficient which is referred to as reflectance in this paper is related to the specific acoustic impedance by

$$R_{\text{\tiny \itshape n}} = \frac{\langle_{\mathsf{S}} \cos_{\text{\tiny \itshape n}} - 1}{\langle_{\mathsf{S}} \cos_{\text{\tiny \itshape n}} + 1}, \tag{7}$$

where $_{\text{\itshape n}}$ is the incident angle. $\langle_{\mathsf{S}} = Z_{\mathsf{S}}/\ldots c$ is the specific acoustic impedance. From inspection of (7), it is clear that the specific acoustic impedance fully characterizes the reflective properties of the boundary for all angles of incidence.

The second boundary is the absorbing boundary conditions (ABCs). Commonly used absorbing boundary models are PML ABC [8] and MUR ABC [9]. As MUR ABC, although successful in many applications, provide only limited absorption to waves within a specific range of incidence angles and frequencies. In the continuous limit, it is proven that a PML interface between a regular medium and such a fictitious perfectly matched medium can completely absorbs incident waves from the regular medium, regardless of its incidence angle and frequency [10]. In this work, the incident wave is wide-band signal, so the PML ABC was used to surround the computational domain.

Ideally, ABCs completely absorb outgoing waves that impinge on the edges of the computational domain. However, since ABCs are imperfect, some nonphysical reflection remains. In some cases, the amount of spurious energy introduced by the ABC can be reduced by adding space between the ABC and the scattered. As seen in Fig. 2, the whole simulation domain is divided into interior region and PML region.
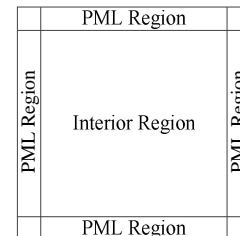

Fig. 2. Computational domain with an interior region and a PML boundary region.

The iterative formula in the PML buffer is as followed [8]:

$$p_x^{n+1}(i,j,k) = e_x^{(1)}(i,j,k) p_x^n(i,j,k) -$$
$$- e_x^{(2)}(i,j,k)[u_x^n(i,j,k) - u_x^n(i-1,j,k)], \tag{8}$$

$$p_y^{n+1}(i,j,k) = e_y^{(1)}(i,j,k)\,p_y^n(i,j,k) -$$
$$-e_y^{(2)}(i,j,k)[u_y^n(i,j,k) - u_x^n(i,j-1,k)], \qquad (9)$$

$$p_y^{n+1}(i,j,k) = e_y^{(1)}(i,j,k)\,p_y^n(i,j,k) -$$
$$-e_y^{(2)}(i,j,k)[u_y^n(i,j,k) - u_x^n(i,j-1,k)], \qquad (10)$$

$$u_x^{n+1}(i,j,k) = e_x^{(3)}(i,j,k)\,u_x^{n+1}(i,j,k) - e_x^{(4)}(i,j,k) \times$$
$$\times [\, p_x^n(i+1,j,k) - p_x^n(i,j,k) + p_y^n(i+1,j,k) -$$
$$-p_y^n(i,j,k) + p_z^n(i+1,j,k) - p_z^n(i,j,k)], \qquad (11)$$

$$u_y^{n+1}(i,j,k) = e_y^{(3)}(i,j,k)\,u_y^{n+1}(i,j,k) - e_y^{(4)}(i,j,k) \times$$
$$\times [\, p_x^n(i,j+1,k) - p_x^n(i,j,k) + p_y^n(i,j+1,k) -$$
$$-p_y^n(i,j,k) + p_z^n(i,j+1,k) - p_z^n(i,j,k)], \qquad (12)$$

$$u_z^{n+1}(i,j,k) = e_z^{(3)}(i,j,k)\,u_z^{n+1}(i,j,k) - e_z^{(4)}(i,j,k) \times$$
$$\times [\, p_x^n(i,j,k+1) - p_x^n(i,j,k) + p_y^n(i,j,k+1) -$$
$$-p_y^n(i,j,k) + p_z^n(i,j,k+1) - p_z^n(i,j,k)], \qquad (13)$$

$$e_x^{(1)}(i,j,k) = \exp(-\mathsf{r}_x(i,j,k)\Delta t \dots c^2), \qquad (14)$$

$$e_x^{(2)}(i,j,k) = (1 - e_x^{(1)}(i,j,k))/(\mathsf{ur}_x(i,j,k)), \quad (15)$$

$$e_x^{(3)}(i,j,k) = \exp(-\mathsf{r}_x(i,j,k)\Delta t), \qquad (16)$$

$$e_x^{(4)}(i,j,k) = (1 - e_x^{(3)}(i,j,k))/(\mathsf{u}\dots\mathsf{r}_x(i,j,k)), \quad (17)$$

$$e_y^{(1)}(i,j,k) = \exp(-\mathsf{r}_y(i,j,k)\Delta t \dots c^2), \qquad (18)$$

$$e_y^{(2)}(i,j,k) = (1 - e_y^{(1)}(i,j,k))/(\mathsf{ur}_y(i,j,k)), \quad (19)$$

$$e_y^{(3)}(i,j,k) = \exp(-\mathsf{r}_y(i,j,k)\Delta t), \qquad (20)$$

$$e_y^{(4)}(i,j,k) = (1 - e_y^{(3)}(i,j,k))/(\mathsf{u}\dots\mathsf{r}_y(i,j,k)), \quad (21)$$

$$e_z^{(1)}(i,j,k) = \exp(-\mathsf{r}_z(i,j,k)\Delta t \dots c^2), \qquad (22)$$

$$e_z^{(2)}(i,j,k) = (1 - e_z^{(1)}(i,j,k))/(\mathsf{ur}_z(i,j,k)), \quad (23)$$

$$e_z^{(3)}(i,j,k) = \exp(-\mathsf{r}_z(i,j,k)\Delta t), \qquad (24)$$

$$e_z^{(4)}(i,j,k) = (1 - e_z^{(3)}(i,j,k))/(\mathsf{u}\dots\mathsf{r}_z(i,j,k)), \quad (25)$$

where r_x, r_y and r_z are the attenuation coefficient in the PML that is introduced artificially in x, y and z direction.

Considering the computation and the absorption effect comprehensively, the PML region is set to 9 grid spaces after many experiments. The attenuation coefficient of each layer is shown in Table I.

TABLE I. ATTENUATION COEFFICIENTS OF PML LAYERS.

PML Layer	Attenuation Coefficients
1	0.0142
2	0.0111
3	0.0083
4	0.0059
5	0.0040
6	0.0024
7	0.0012
8	0.0005
9	0.0001

III. IMPROVED METHOD

A. Frequency-dependent Iterative Equation

The above equations are appropriate for homogeneous non-dissipative medium, but in the actual situation, there are many factors should be considered.

When sound propagates in the sea, the absorption of sound is mainly through two mechanisms: viscous absorption and molecular thermal relaxation absorption. Absorption loss is related to frequency. The whole absorption loss can be represented by the absorption coefficient s (dB/KYD). The formula is as followed [11]

$$\mathsf{s} = \frac{0.102 f^2}{1 + f^2} + \frac{40.7 f^2}{4100 + f^2} + 2.75 \times 10^{-4} f^2 + $$
$$+ 0.003, \qquad (26)$$

where f is frequency, the unit is kHz.

The acoustic attenuation coefficient of a wide range of viscoelastic materials can be expressed as the following power law with respect to frequency [10]

$$p(r + \Delta r) = p(r)e^{-\mathsf{s}\Delta r}, \qquad (27)$$

where Δr is transmission distance. Because the FDTD iterative formula is by the time, so $\Delta r = c \cdot \Delta t$.

When $\Delta x = \Delta y = \Delta z = c \cdot \Delta t$, the modified FDTD formulas that consider the frequency dependent absorption coefficient are followed as:

$$u_x^{(n)}(i,j,k) = \{u_x^{(n-2)}(i,j,k) -$$
$$-\frac{\Delta t}{\mathsf{u}\dots}[\, p^{(n-1)}(i+1,j,k) -$$
$$-p^{(n-1)}(i-1,j,k)]\} \times e^{-\mathsf{s}\Delta x}, \qquad (28)$$

$$u_y^{(n)}(i,j,k) = \{u_y^{(n-2)}(i,j,k) -$$
$$-\frac{\Delta t}{\mathsf{u}\dots}[\, p^{(n-1)}(i,j+1,k) -$$
$$-p^{(n-1)}(i,j-1,k)]\} \times e^{-\mathsf{s}\Delta y}, \qquad (29)$$

$$u_z^{(n)}(i,j,k) = \{u_z^{(n-2)}(i,j,k) -$$
$$-\frac{\Delta t}{\mathsf{u}\dots}[\, p^{(n-1)}(i,j,k+1) -$$
$$-p^{(n-1)}(i-1,j,k-1)]\} \times e^{-\mathsf{s}\Delta z}, \qquad (30)$$

$$up^{(n)}(i,j,k) = \{p^{(n-2)}(i,j,k) -$$
$$-\frac{\dots c^2 \Delta t}{\mathsf{u}}[u_x^{(n-1)}(i+1,j,k) -$$
$$-u_x^{(n-1)}(i-1,j,k) + u_y^{(n-1)}(i,j+1,k) -$$
$$-u_y^{(n-1)}(i,j-1,k) +$$
$$+u_z^{(n-1)}(i,j,k+1) - u_z^{(n-1)}(i,j,k-1)]\} \times e^{-\mathsf{s}\,c\Delta t}, \qquad (30)$$

$$p^{(n)}(i,j,k) = \{p^{(n-2)}(i,j,k) -$$
$$-\frac{\dots c^2 \Delta t}{\mathsf{u}}[u_x^{(n-1)}(i+1,j,k) -$$

$$-u_x^{(n-1)}(i-1,j,k) + u_y^{(n-1)}(i,j+1,k) -$$
$$-u_y^{(n-1)}(i,j-1,k) +$$
$$+u_z^{(n-1)}(i,j,k+1) - u_z^{(n-1)}(i,j,k-1)]\} \times e^{-S c \Delta t}. \quad (31)$$

Usually, U should be sufficiently small, generally one tenth of the wavelength or less. Since the input sound source is wide-band signal, the wavelength should be selected the smallest wavelength of the signal. In the whole calculation field, there are two media, c_1 is the sound speed in water, c_2 is the sound speed in the object ($c_2 > c_1$).

Considering calculation speed and accuracy, the revised stability condition is:

$$\leq \frac{1}{10} \}_{\min} = \frac{1}{10} \frac{c_1}{f_{\max}}, \quad (32)$$

$$\Delta t \leq \frac{\mathsf{u}}{\sqrt{3} c_2}, \quad (33)$$

where $\}_{\min}$ and $f_{\max}$ are the smallest wavelength and the maximum frequency of the broadband signal, respectively.

B. Mesh-generating Method of Complex Object

In order to simulate acoustic scattering of irregular object, the target need to be gridded. The stretched mesh [12] is an effective way to improve calculation accuracy, but it requires huge memory and computing time. Some grid processing based on the cylindrical coordinate system is simple, but the iterative formulas will become more complicated [13]. Computer Graphics are also used to mesh-generating of FDTD method, which is easy to understand and requires less memory to achieve.

3DMAX software is utilized to generate the complex object, then export an ASE format file. By processing the file, FDTD mesh-generating is realized.

The ASE file includes much information, such as the numbers of faces, face material, vector of vertices and so on. In order to filter the useless information in ASE file and extract useful data, data extraction process is in demand. Processing flow is as shown in Fig. 3.

Scan ASE data file

Obtain the information value of the triangle side

cycling scan point data information

cycling scan surface data information

three-dimensional coordinates of the surface three vertexes

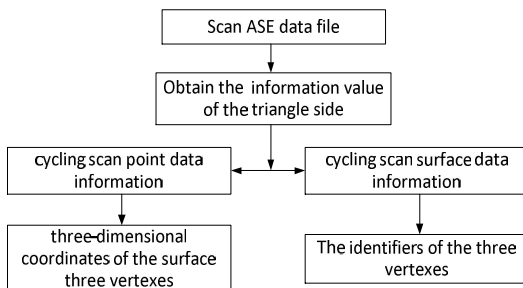The identifiers of the three vertexes

Fig. 3. Data processing flow chart.

To judge the position relationship of the grid centre and the target model, the model is divided into a finite number of tetrahedron. Each tetrahedron is made up of three vertices of the triangle patch and centre of model. So just determine relations of the centre of each cell with tetrahedron of the model. The key is how to determine the spatial relationship

between any point and the location of the tetrahedron. Figure 4 shows a tetrahedron ABCD and any point P in space. A, B and C are the three vertices of any triangle patch, the coordinates are (x_1, y_1, z_1), (x_2, y_2, z_2) and (x_3, y_3, z_3). D is the centre of model, which coordinate is (x_0, y_0, z_0). The coordinates of P can be written as ($\sum_{i=0}^{3} v_i x_i$, $\sum_{i=0}^{3} v_i y_i$, $\sum_{i=0}^{3} v_i z_i$) and $\sum_{i=0}^{3} v_i = 1$:

$$v_0 = \frac{\vec{n}_0 \cdot (\vec{P} - \vec{C})}{\vec{n}_0 \cdot (\vec{D} - \vec{C})}, \quad (34)$$

$$v_1 = \frac{\vec{n}_1 \cdot (\vec{P} - \vec{B})}{\vec{n}_1 \cdot (\vec{A} - \vec{B})}, \quad (35)$$

$$v_2 = \frac{\vec{n}_2 \cdot (\vec{P} - \vec{A})}{\vec{n}_2 \cdot (\vec{B} - \vec{A})}, \quad (36)$$

$$v_4 = \frac{\vec{n}_3 \cdot (\vec{P} - \vec{D})}{\vec{n}_3 \cdot (\vec{C} - \vec{D})}. \quad (37)$$

where $\vec{n}_0$, $\vec{n}_1$, $\vec{n}_2$ and $\vec{n}_3$ are the normal lines of planes ABC, BCD, ACD and ABD in the tetrahedron ABCD. If $v_1 \geq 0$, $v_2 \geq 0$, $v_3 \geq 0$, $v_4 > 0$, then P is in the target model, if $v_1 \geq 0$, $v_2 \geq 0$, $v_3 \geq 0$, $v_4 = 0$, then P is on the surface of the target model. If one of v_1, v_2, v_3 and v_4 is less than zero, P is out of the tetrahedron and then compare with other tetrahedron.
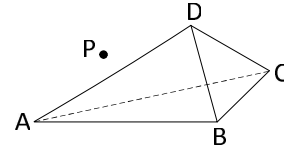
Fig. 4. The position of a tetrahedron and any point.

Finally, three matrices are generated as the grid data. One is the interior points of the object, another is the surface points of the object, the other is the whole points of the object.

IV. SIMULATION RESULTS AND ANALYSIS

In our simulation, sound speed and density of water are set to 1500 m/s and 1025 kg/m^3, respectively. Sound speed and density of sediment are 4500 m/s and 2700 kg/m^3, $\Delta t = 0.0056 \, \text{ms}$.

A. Simulation Using Single Frequency Signal

A single frequency sinusoidal signal which frequency is 1.5 kHz and pulse width is 4.44 ms is used as the incident wave. The radius of the circle is 1.5 m. The simulation result is shown in Fig. 5.

Figure 5(a) is the simulation result using FDTD algorithm in this paper. Figure 5(b) is the result using Wang's method with the first-order Mur's ABC in paper [6]. From Fig. 5, it can be seen that the scattered fields of two methods are almost the same. Because of different boundary conditions, the results are not the quite the same. In Fig. 5(a), the incident wave transmit into the circle, then penetrate the object and go

on propagating forward. So diffraction wave in Fig. 5(a) is more obvious. Through this comparison, the method proposed in this paper is proved to be correct. The spectrums of the incident wave and the scattered wave are shown in Fig. 6.
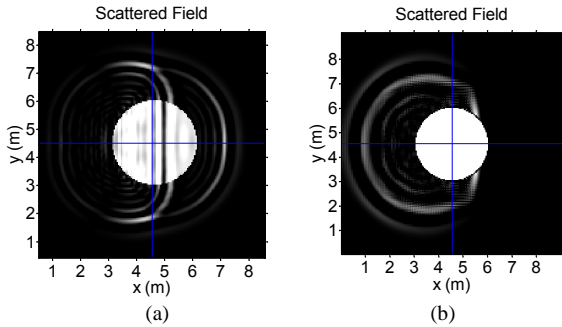

Fig. 5. Scattered field when incident wave is single frequency signal: a) Our result, (b) Wang's result.
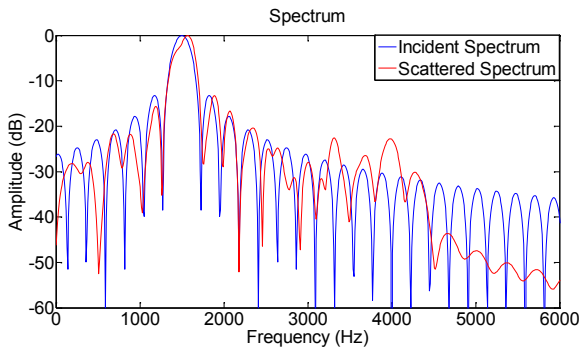

Fig. 6. Comparison on the spectrum of incident wave and scattered wave.

The scattered wave is taken from the location (1 m, 2 m) of computation field. Obviously, it can be seen from Fig. 6 that some new frequency components showed up in the scattered waves. It means that there is the dispersion in sound propagation.

B. Incidence Wave

Linear Frequency Modulation (LFM) signal has a good resistance to interference, multipath effect and Doppler frequency shift, and is widely applied in sonar, radar and other fields. So LFM pulse is used as the incidence wave.

The expression of LFM signal is

$$f(t) = p_0 \exp\left[2\ \mathrm{j}(f_0 + Kt)t\right], \tag{38}$$

where f_0 and p_0 is the starting frequency and acoustic pressure at $t = 0$, and K is the rate of frequency increase or chirp rate. In simulation, $f_0 = 1.5\mathrm{kHz}$, $p_0 = 1$, $K = 2 \times 10^5$ Hz/s, and pulse width of the LFM signal is 4.18 ms.

C. Scattering from Circle in 2D

The FDTD algorithm is first applied to a circle in 2D.

Figure 7 illustrates the grey scale image of the incident wave and the object. It can be seen that the calculation field is a 9 m × 9 m square space. Incidence wave is set at the line where is $x = 0.5$ m. Plane incident wave comes from the left. The instantaneous pressure values of the plane wave are visualized by different grey levels, with the intermediate grey shade representing zero, and the darker and brighter shades representing negative and positive excursions, respectively. The brighter shade is becoming denser and denser, this

indicates the frequency is increasing. It is in accord with the LFM waveform. It is shown in Fig. 8 that the instantaneous pressure distribution of the scattered field and the total field around the circle at time $t = 6.67$ ms. The solid circle is at the centre of the rectangular region. The circle is insonified by a plane incident wave from the left. A Cartesian coordinate system is used. It can be seen from the diagram that there are more cycles than the incident wave, because the incident wave gradually disappears, just like when we drum, the sound disappears after a while.
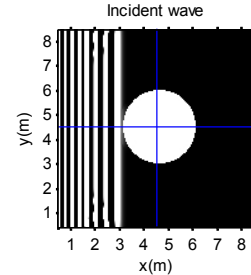

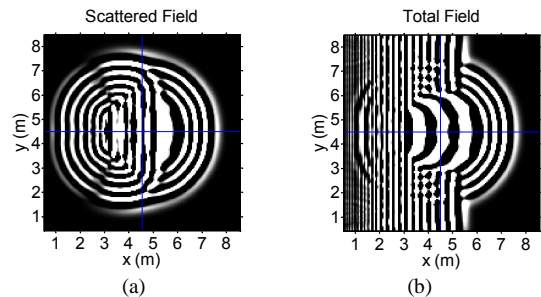Fig. 7. Incident wave is about to hit the circle.

Fig. 8. Distribution of pressure magnitude: a) the scattered field, b) the total field.

D. Scattering from Complicated Object in 3D

A complex object is generated by 3DMAX, as shown in Fig. 9. The total calculation field is a 9 m × 9 m × 9 m cubic space. The object's centre coordinates is (4.5 m, 4.5 m, 4.5 m). Incidence wave is set at the YOZ plane $x = 0.5$m. Figure 10 illustrates the gridding result by mesh-generating method.
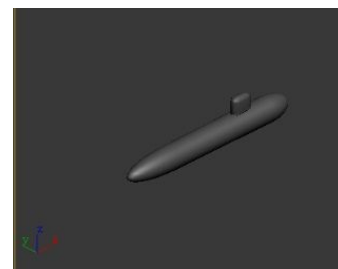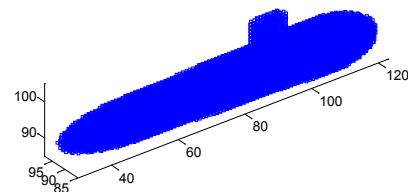

Fig. 9. Irregular object.

Fig. 10. Gridding result.

The incident wave in XOY plane and XOZ plane is shown in Fig. 11. In XOY plane, the shadow of the object is symmetrical, as shown in Fig. 11(a). From Fig. 11(b), we can see that the object is not symmetrical. Figure 11 visualizes the

instantaneous pressure distribution obtained by FDTD at $t = 1.23$ ms. In this moment, the incident is about to hit the object. The distribution of the pressure magnitude of scattered field and total field is present in Fig. 12 and Fig. 13.
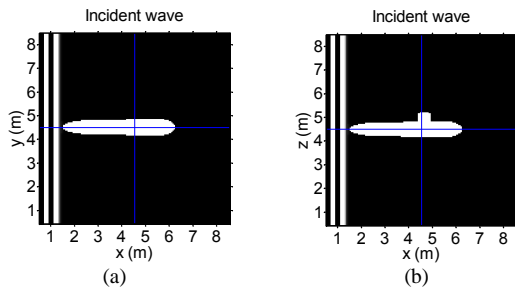

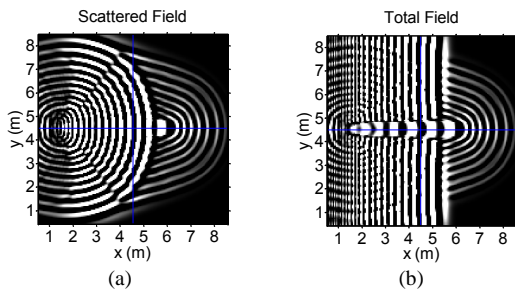Fig. 11. LFM pulse is propagating in the positive x direction: a) in XOY plane, b) in XOZ plane.

Fig. 12. Distribution of sound pressure at t = 6.67 ms (XOY plane): a) the scattered field, b) the total field.

From the plots, the incident wave is also propagating into the object, this is the result of impedance ABC. The wave speed in the object is faster than in the water. Compared Fig. 12(a) with Fig. 13(a), it can be seen that they all have obvious diffraction. Different from the diffraction in Fig. 12(a), it is not symmetrical in Fig. 13(a). This is because of the bulge of the object in XOZ plane. The sound pressure of any point in the field can be obtained, as shown in Fig. 14.
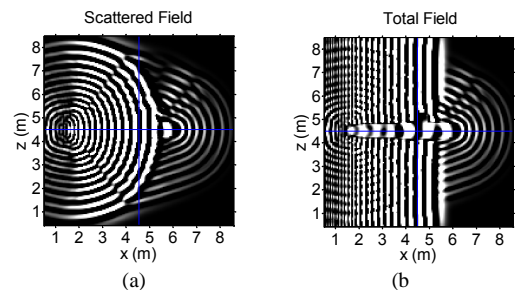

Fig. 13. Distribution of sound pressure at t = 6.67 ms (XOZ plane), a) the scattered field, b) the total field.

In Fig. 14, it is the waveforms of certain point in the calculation field. The three points are in the same line. First, in Fig. 14(a) and Fig. 14(b), There is both obvious attenuation as the wave's propagation. In Fig. 14(c), there is also attenuation at the last, but it is not obvious. This is due to the limit of displaying time. If the timeline is longer, there is obvious attenuation too. The receiving point of Fig. 14(a) and Fig. 14(c) are axisymmetric. In the two figures, scattering sound waves reach at the same moment $t = 4.0$ ms. In Fig. 14(b), the wave reaching time is $t = 1.6$ ms. Though scattering sound waves reach at the same moment of Fig. 14(a) and Fig. 14(c), there is still difference in decay rate of this two figures. Figure 14(c) has a wider waveform

because of the bulge of the object in XOZ plane. The waveform indicates the shape characteristics of the object.
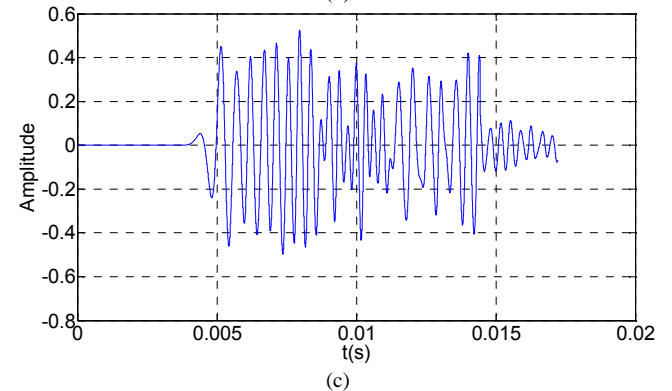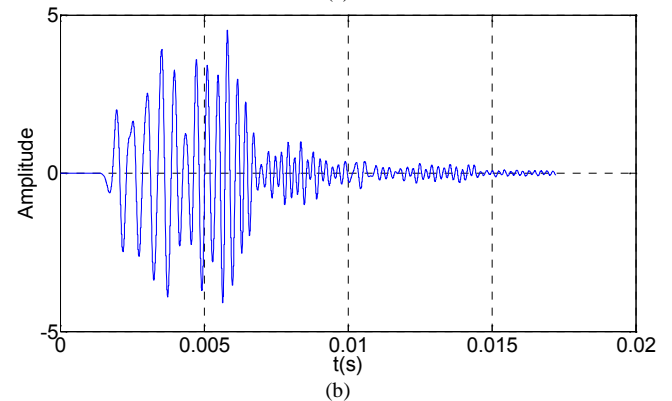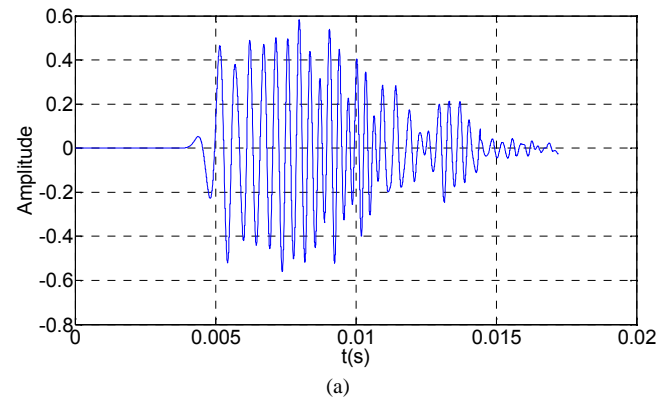

Fig. 14. The scattered acoustic pressure waveform, a) at point (1 m, 4.5 m, 2 m), b) at point (1 m, 4.5 m, 4.5 m), c) at point (1 m, 4.5 m, 7 m).

V. CONCLUSIONS

A modified FDTD method is described in this paper. The absorption coefficient which is frequency-dependent is considered, and it is applied to calculating broadband acoustic scattering model of underwater complex object. The object is with penetrable interface that has finite acoustic impedance. PML absorbing boundary conditions is used in the computation. The boundary conditions are effectively. In order to solve the difficult problem of 3D irregular target modelling in the acoustic calculation with the FDTD method, the mesh-generating approach in electromagnetism is applied to underwater acoustic. The principle of this method is to judge whether the centre of Yee cell is in or on the target model. The result demonstrates that an auto grid splitting of FDTD method is exactly and quickly achieved by this method. Numerical results using LFM wide-band signal pulse as the incidence wave are presented for scattering from simple circle in 2D to complex object in 3D. Compared with

other FDTD articles [6], the proposed method is correct and effective when a single-frequency signal is used as incident wave. On this basis, after considering frequency-dependent absorption attenuation, simulation results for broadband transient problems are made closer to the actual.

This new algorithm is a progress in computing underwater acoustic problem. The simulation data can be used to conduct DOA estimation. That is a part of our present research.

REFERENCES

[1] K. S. Yee, "Numerical solution of initial boundary value problems involving Maxwell's equations in isotropic media", *IEEE Trans. On Antennas and Propagation*, vol. 14, no. 3, pp. 302–307, 1966. [Online]. Available: http://dx.doi.org/10.1109/TAP.1966.1138693

[2] D. Botteldooren, "Finite-difference time-domain simulation of low-frequency room acoustic problems", *The Journal of the Acoustical Society of America*, vol. 98, no. 6, pp. 3302–3308, 1995. [Online]. Available: http://dx.doi.org/10.1121/1.413817

[3] K. Kowalczyk, M. Walstijn, "Modeling frequency-dependent boundaries as digital impedance filters in FDTD and K-DWM room acoustics simulations", *Journal of the Audio Engineering Society*, vol. 56, no. 7/8, pp. 569–583, 2008.

[4] T. Sun, G. Li, K. Wang, "A near-to-far-field transformation method for acoustic scattering problems", in *Proc. (ICMA 2007)*, 2007, pp. 304–308.

[5] J. J. Lopez, J. M. Navarro, D. Carnicero, *et al.*, "Some comments about graphic processing unit architectures applied to finite-difference time-domain room acoustics simulation: Present and future trends", *The Journal of the Acoustical Society of America*, 2013, vol. 133, no. 5, pp. 3614–3620. [Online]. Available: http://dx.doi.org/10.1121/1.4806744

[6] S. Wang, "Finite-difference time-domain approach to underwater acoustic scattering problems", *The Journal of the Acoustical Society of America*, pp. 1924–1931, 1996. [Online]. Available: http://dx.doi.org/10.1121/1.415375

[7] H. Saito, J. Naoi, T. Tsuchiya, *et al.* "Application of the finite difference time domain method to the time reversal wave in shallow water", in *Proc. of Oceans 2004, MTTS/IEEE TECHNO-OCEAN'04*, vol. 4, pp. 2236–2241.

[8] H. K. Z. Yue-zhe, "Attenuation ability influenced by amount and attenuation coefficient of perfectly-matched layers in acoustic FDTD method", *Journal of South China University of Technology (Natural Science Edition)*, vol. 39, no. 4, pp. 135–139, 2011.

[9] F. Liang, G. Wang, H. Lin, *et al.*, "Mur absorbing boundary condition for three-step 3-D LOD-FDTD method", *IEEE Microwave and Wireless Components Letters*, vol. 20, no. 11, pp. 589–591, 2010. [Online]. Available: http://dx.doi.org/10.1109/LMWC.2010.2072916

[10] W. Chen, S. Holm, "Modified Szabo's wave equation models for lossy media obeying frequency power law", *The Journal of the Acoustical Society of America*, 2003, vol. 114, no. 5, pp. 2570–2574. [Online]. Available: http://dx.doi.org/10.1121/1.1621392

[11] R. J. Urick, *Principles of Underwater Sound.* McGraw-Hill, 1996, pp. 103–110.

[12] J. Berenger, F. Costen, H. Almeer, "The stretched-mesh huygens absorbing boundary condition (SM-HABC)", *IEEE Trans. on Antennas and Propagation*, 2014, vol. 62, no. 6, pp. 3100–3107. [Online]. Available: http://dx.doi.org/10.1109/TAP.2014.2314295

[13] O. Markish, R. Kastner, "Cylindrical FDTD grid-compatible Green's functions", *Journal of Computational Physics*, 2013, vol. 240, pp. 198–210. [Online]. Available: http://dx.doi.org/10.1016/j.jcp.2012.12.011

[14] J. H. Ehrlich, "Time domain modeling of acoustic propagation with acoustic wave propagator and absorbing boundary conditions", *Journal of the Acoustical Society of America*, vol. 123, no. 5, pp. 3530–3534, 2008. [Online]. Available: http://dx.doi.org/10.1121/1.2934481